Second-harmonic interferometric spectroscopy of the buried Si(111)-SiO_2 interface

A.A. Fedyanin, T.V. Dolgova, O.A. Aktsipetrov

Department of Physics, Moscow State University, 119899 Moscow, Russia

D. Schuhmacher, G. Marowsky

Laser-Laboratorium Göttingen, Hans-Adolf-Krebs-Weg 1, D-37077 Göttingen, Germany

Abstract

The second-harmonic interferometric spectroscopy (SHIS) which combines both amplitude (intensity) and phase spectra of the second-harmonic (SH) radiation is proposed as a new spectroscopic technique being sensitive to the type of critical points (CP's) of combined density of states at semiconductor surfaces. The increased sensitivity of SHIS technique is demonstrated for the buried Si(111)-SiO_2 interface for SH photon energies from 3.6 eV to 5 eV and allows to separate the resonant contributions from E_0'/E_1, E_2 and E_1' CP's of silicon.

Second-harmonic generation (SHG) is inherently sensitive to surface and interface properties of centrosymmetric materials. Recently, the spectroscopy of the second-harmonic (SH) intensity has been proved as a promising probe of surfaces and interfacial layers[1] and intensively employed in numerous works for oxidized[2], reconstructed[3] and H-terminated[4] silicon surfaces. The resonances of the SH intensity are attributed in these cases to direct interband electron transitions. By analogy with the spectrum of the linear dielectric function $\varepsilon(\omega)$ the spectrum of the quadratic susceptibility $\chi^{(2)}(2\omega)$ of such semiconductor surfaces could be expressed as the superposition of several van Hove singularities (critical points (CP's) of the combined density of states) $\chi^{(2)}_m(2\omega) \propto (2\omega - \omega_m + i\Gamma_m)^n$ with threshold frequencies ω_m and broadenings Γ_m[5]. The exponent n reflects the dimensionality of CP: $n = 1/2, 0$

(logarithmic), $-1/2, -1$ for 3D, 2D, 1D and excitonic CP, respectively. Although the line shapes $\chi^{(2)}(2\omega)$ are quite different for various n, in most cases a large number of adjustable parameters makes the determination of the type of CP solely from the SH intensity spectrum doubtful, and most of authors interpret the SHG spectroscopy data within excitonic CP line shape[6].

The single-beam SH interferometry traces back to the mid-1960s[8] and is conventionally used for the determination of the phase of the quadratic susceptibility of adsorbate molecules and their absolute direction[9] and for separation of the SH contributions from thin films and their substrates[10]. Another use of SH phase measurements is a homodyne mixing technique to improve the signal-to-noise ratio for surface SHG probe[11]. The use of external[12] and internal[13] homodynes for dc or low-frequency modulated electric-field-induced SHG allows to measure the in-plane spatial distribution of the electric field vector with micron resolution or to visualize weak nonlinear contributions. Further developments of the SH interferometry are the frequency-domain interferometric SH spectroscopy[14] exploring the broad bandwidth of femtosecond laser pulses, and the hyper-Rayleigh scattering interferometry[15] using the correlation of fluctuations in linear and nonlinear optical properties of thin inhomogeneous films.

In this Letter, a modification of the SH spectroscopy - the SH interferometric spectroscopy (SHIS) which combines both amplitude (intensity) SH spectroscopy and SH interferometry is proposed. The combination of the phase and amplitude SH spectra, extracted from the SHIS data, is shown to be sensitive to type of CP even for systems with interfering SH contributions from close electronic resonances. Additionally SHIS allows to avoid the sign uncertainty of $\mathrm{Re}(\chi^{(2)})$ inherent in the conventional spectroscopy of the SHG intensity. The spectral dependence of the phase and amplitude of the SH waves from the buried Si(111)-SiO_2 interface is measured using the SHIS technique in the spectral range in the vicinity of silicon E_2 CP. In contrast to E_0'/E_1 CP revealing the excitonic type, the family of E_2 CP's of the bulk silicon demonstrates the 2D type in linear response[7]. The resonant contributions to the quadratic susceptibility from E_0'/E_1, E_2 and E_1' silicon CP's are extracted

within the simple phenomenological model which accounts the complex Green's function corrections for the SH wave generation.

The scheme of the SHIS setup is shown in Fig.1(a). The p-polarized output of a tunable nanosecond parametric generator/amplifier laser system (Spectra-Physics MOPO 710) operating in the interval of 490 - 690 nm is focused onto the sample at an angle of incidence of 45°. The SH signal is detected by a monochromator, a photomultiplier tube (PMT) and an electronic peak-hold detector. To normalize the SH intensity spectrum over the laser fluence and the spectral sensitivity of the optical detection system a SHG intensity reference channel is used with a slightly wedged z-cut quartz plate and with the detection system identical to the one in the sample channel. The (phase-)reference sample is chosen (i) to be thin enough to avoid Maker fringes in the SH response during tuning the fundamental wavelength λ_ω, (ii) to be optical inactive for conservation the polarization state of the fundamental radiation while transmitting through it, (iii) to have no resonance features in the tuning region of both the fundamental and SH waves. Therefore the 1 mm-thick plate of fused quartz coated with a 30 nm-thick indium tin oxide (ITO) film is chosen as a reference. The SH interferogram is obtained by translating the reference along the fundamental laser beam varying the distance l between the reference and the sample. The SH signals from the reference, $I_r^{2\omega}$, and from the sample, $I_s^{2\omega}$, are monitored separately by inserting appropriate filters (yellow or UV, respectively) between the reference and the sample. $I_r^{2\omega}$ is adjusted with the angle of incidence of the fundamental beam at the ITO phase reference. The detected SH intensity $I^{2\omega}$ is the result of interference of the SH waves from the reference, $E_r^{2\omega}$, and from the sample, $E_s^{2\omega}$:

$$I^{2\omega} = \frac{c}{8\pi}|E_r^{2\omega}(l) + E_s^{2\omega}|^2 = I_r^{2\omega}(l) + I_s^{2\omega} + 2\alpha\sqrt{I_r^{2\omega}(l)I_s^{2\omega}}\cos\left(2\pi\frac{l}{L} + \Phi_{rs}\right), \qquad (1)$$

where $L = \lambda_\omega(2\Delta n)^{-1}$ is the period of SH interferogram with $\Delta n = n_{2\omega} - n_\omega$ describing the air dispersion, and $\alpha < 1$ indicates the laser coherence. The position-dependent phase shift $2\pi l/L$ between $E_r^{2\omega}$ and $E_s^{2\omega}$ comes from the different refractive indices of air for the fundamental and SH waves. The spectral dependences of $\chi^{(2)}$ of the reference and the

sample as well as the complex Green's function corrections for the SH wave produce a position-independent phase shift $\Phi_{rs}(\lambda_\omega, \lambda_{2\omega})$. The dependence $I_r^{2\omega}(l)$ is described by the conventional formula for focused Gaussian beams. The spectrum of the phase of the SH wave from the ITO film, $\Phi_r \equiv \mathrm{Arg}(E_r^{2\omega})$, is measured using the 1 mm-thick backside-immersed y-cut quartz as a sample since the phase of the SH wave from the quartz surface is spectrally independent in the whole used spectral region. The Φ_r spectrum of the ITO film appears to be a constant within the error bars and $I_r^{2\omega}$ gradually increases with decreasing λ_ω without any resonance features.

The samples are natively oxidized p-doped Si(111) wafers with resistivity of $10\Omega \cdot cm$. SHIS has been performed at the maximum of the azimuthal SH rotational anisotropy for the p-in, p-out polarization combination of the fundamental and SH waves. Figure 1(b) shows typical SH interference patterns measured for different λ_ω. The spectral dependence of the period L due to the air dispersion and clear changes in the contrast of the patterns due to the distance dependence of $I_r^{2\omega}$ in the focused laser beam are seen. The fit of the set of SH interference patterns by Eq.(1) with Φ_{rs}, $I_s^{2\omega}$, L, and α as adjustable parameters leads to the spectra of Φ_{rs}, $I_s^{2\omega}$ and L shown in Fig. 2(a) and 2(b) and in the inset of Fig. 1, respectively. To emphasize the spectral features of $I_s^{2\omega}(2\omega)$, we combine the fitted intensity spectrum with the $I_s^{2\omega}(2\omega)$ dependence measured directly with a fine resolution in SH photon energy. Φ_{rs} increases approximately by 1.2 radians within the interval of 4.2-4.6 eV and decreases outside this energy region. A small, but reliable, non-monotonic feature is seen at 3.8 - 4.0 eV. The $I_s^{2\omega}$ spectrum has pronounced peaks centered approximately at 3.9 eV and 4.3 eV. The position of the 4.3 eV resonance is close to E_2 CP and we associate the observed features of SH phase and intensity spectra for energies between 4.1 and 4.6 eV with direct interband electron transitions at E_2 CP of Si[7].

The relative phase Φ_{rs} measured in SHIS is given by:

$$\Phi_{rs} = \Phi_s - (\Phi_r + \mathrm{Arg}(R_{2\omega})), \tag{2}$$

where $R_{2\omega}$ is the Fresnel reflection factor of the p-polarized SH radiation from the Si-SiO_2

interface. The phase $\Phi_s \equiv \mathrm{Arg}(E_s^{2\omega})$ originates from both complex surface $\chi^{(2),S}$ and bulk quadrupole $\chi^{(2),BQ}$ quadratic susceptibilities as well as from Green's function corrections[16]:

$$E_s^{2\omega} = G_\| \chi_\|^{(2)} + G_\perp \chi_\perp^{(2)}, \tag{3}$$

where $G_\|$ and $G_\perp$ are the Green's function corrections for the generation and the propagation of in-plane and normal components of $E_s^{2\omega}$, and $\chi_\|^{(2)}$ and $\chi_\perp^{(2)}$ are the corresponding effective components of $\chi^{(2)}$. $\chi_\|^{(2)}$ and $\chi_\perp^{(2)}$ are the linear combinations of $\chi^{(2),S}$ and $\chi^{(2),BQ}$ components with nonresonant coefficients depending only on the fundamental wavevector and taking into account the geometry of the nonlinear interaction. This allows to consider the spectral dependences of $\chi_\|^{(2)}$ and $\chi_\perp^{(2)}$ as a superposition of two-photon resonances for different CP's:

$$\chi_\alpha^{(2)}(2\omega) = B - \sum_m f_m^\alpha \exp(i\phi_m^\alpha)(2\omega - \omega_m + i\Gamma_m)^n, \tag{4}$$

where $\alpha = \perp, \|$, and m numerates the CP resonances. The oscillator strengths f_m^α are supposed to be real numbers. For the sake of simplicity, a slight spectral dependence of the term B including the Si resonances with threshold energies below 1.5 eV[3] is neglected, and ϕ_m^α are integer multiples of $\pi/2$ defining the type of CP. The solid lines in Fig.2 show the fit of Φ_{rs} and $I_s^{2\omega}$ spectra by Eq.(2) and $|E_s^{2\omega}|^2$ from Eq.(3), respectively, with the Si dispersion data from Ref.[17] and expressions for $G_\|$ and $G_\perp$ from Ref.[18]. Five resonant contributions are included into the fit. The first resonance, centered at $\omega_1 = 3.45$ eV, has excitonic line shape ($n = -1, \phi_1 = 0$) and corresponds to the direct electron transitions at E_0'/E_1 CP. The second resonance at 3.97 eV with 1D maximum line shape ($n = -1/2, \phi_2 = 0$) has no equivalent in the band structure of crystalline bulk silicon. However, a resonance in the close energy interval has been recently observed at the Si(001)-SiO_2 interface[6] and could be associated with transition in Si atoms located at the interface with reduced lattice symmetry. The strong resonant features in the vicinity of 4.3 eV are formed by interference of two resonances centered at $\omega_3 = 4.12$ eV and at $\omega_4 = 4.34$ eV with almost equal amplitudes ($f_4 \approx 0.9 f_3$). It is mostly reasonable to attribute these peaks to transitions at $E_2(X)$ and $E_2(\Sigma)$ CP's. These resonances are fitted with 2D minimum ($\phi_3 = 0$) and 2D maximum

($\phi_4 = \pi$) line shapes ($\chi^{(2)}_m \propto \ln(2\omega - \omega_m + i\Gamma_m)$) by analogy with the linear case[7]. Note, that ω_3 and ω_4 are approximately 0.1 eV red-shifted from resonances of linear $\chi^{(1)}$. This allows to interpret also 4.12 eV-resonance as a contribution from E_0 CP, which is normally very weak in the linear response. The best representation of the data is obtained with a 2D minimum line shape of the last resonance, centered at 5.15 eV, which can be associated with electron transitions located near E_1' CP[7]. The error bars for the central frequencies are approximately 0.03 eV and mostly attributed to the relative weight of $\chi^{(2)}_{\parallel}$ and $\chi^{(2)}_{\perp}$ being unresolvable from our data. Excitonic line shapes for all resonances (dotted lines in Fig.2) fit the $I_s^{2\omega}$ spectrum with almost the same quality as the CP model, but fit the Φ_{rs} spectrum obviously worse.

Summarizing, the general scheme of the second-harmonic interferometric spectroscopy is presented. The phase and amplitude of the SH wave from the buried Si(111)-SiO_2 interface are measured simultaneously using the SHIS technique in the interval of SH photon energies from 3.6 eV to 5 eV. The contributions of interband transitions located at E_0'/E_1, E_2 and E_1' Si critical points are separated and sensitivity of SHIS to CP line shapes is shown.

This work was supported by the Russian Foundation for Basic Research (RFBR) and Deutsche Forschungsgemeinschaft (DFG): RFBR grant 98-02-04092, DFG grants 436 RUS 113/439/0 and MA 610/20-1, RFBR grant 00-02-16253, special RFBR grant for Leading Russian Science Schools 00-15-96555; NATO Grant PST.CLG975264, Russian Federal Program "Center of Fundamental Optics and Spectroscopy", and Program of Russian Ministry of Science and Technology "Physics of Solid State Nanostructures".

REFERENCES

1. T. F. Heinz, in: *Nonlinear Surface Electromagnetic Phenomena*, Eds. H. -E. Ponath and G. I. Stegeman (Elsevier Publ. Co., Amsterdam 1991), p. 353; J. F. McGilp, Phys. Status Solidi A **175**, 153 (1999); G. Lüpke, Surf. Sci. Rep. **35**, 75 (1999).

2. W. Daum, H.-J. Krause, U. Reichel, and H. Ibach, Phys. Rev. Lett. **71**, 1234 (1993).

3. K. Pedersen and P. Morgen, Phys. Rev. B **53**, 9544 (1996).

4. J. I. Dadap, N. M. Russel, Z. Xu, X. F. Hu, J. G. Eckerd, O. A. Aktsipetrov, and M. C. Downer, Phys. Rev. B **56**, 13367 (1997).

5. M. Cardona, *Modulation Spectroscopy*, Suppl. 11 of *Solid State Physics*, edited by F. Seitz, D. Turnbull, and H. Ehrenreich (Academic, New York 1969), chap. 2.

6. G. Erley and W. Daum, Phys. Rev. B **58**, R1734 (1998); G. Erley, R. Butz, and W. Daum, Phys. Rev. B **59**, 2915 (1999).

7. P. Lautenschlager, M. Garriga, L. Vina, and M. Cardona, Phys. Rev. B **36**, 4821 (1987).

8. R. K. Chang, J. Ducuing, N. Bloembergen, Phys. Rev. Lett. **15**, 6 (1965).

9. K. Kemnitz, K. Bhattacharyya, J. M. Hicks, G. R. Pinto, K. B. Eisenthal, T.F. Heinz, Chem. Phys. Lett. **131**, 285 (1986).

10. R. Stolle, G. Marowsky, E. Schwarzberg, G. Berkovic, Appl. Phys. B **63**, 491 (1996).

11. P. Thiansathaporn and R. Superfine, Opt. Lett. **20**, 545 (1995); J. Chen, S. Machida, and Y. Yamanoto, Opt. Lett. **23**, 676 (1998).

12. J. I. Dadap, J. Shan, A. S. Weling, J. A. Misewich, A. Nahata, and T. F. Heinz, Opt. Lett. **24**, 1059 (1999).

13. O. A. Aktsipetrov, A. A. Fedyanin, A. V. Melnikov, E. D. Mishina, A. N. Rubtsov, M. H. Anderson, P. T. Wilson, M. ter Beek, X. F. Hu, J. I. Dadap, and M. C. Downer,

Phys. Rev. B **60**, 8924 (1999).

14. P. T. Wilson, Y. Jiang, O. A. Aktsipetrov, E. D. Mishina, and M. C. Downer, Opt. Lett. **24**, 496 (1999).

15. A. A. Fedyanin, N. V. Didenko, N. E. Sherstyuk, A. A. Nikulin, and O. A. Aktsipetrov, Opt. Lett. **24**, 1260 (1999).

16. P. Guyot-Sionnest, W. Chen, and Y. R. Shen, Phys. Rev. B **33**, 8254 (1986).

17. D. E. Aspnes and A. A. Studna, Phys. Rev. B **27**, 985 (1983).

18. O. A. Aktsipetrov, T. V. Dolgova, A. A. Fedyanin, D. Schuhmacher, G. Marowsky, Thin Solid Films **364**, 91 (2000).

FIGURES

Fig. 1. Panel a: Experimental setup for the SH interferometric spectroscopy. BS, beam splitter; GG and UG, yellow and UV filters, respectively. Panel b: Raw SH interferograms for different SH energies. Solid curves: The dependences given by Eq.(1). Inset: The spectral dependence of the period L of the SH interferograms and its fit using a phenomenological expression for air dispersion. Open circles indicate the periods for the curves at the main panel.

Fig. 2. Spectrum of the SH phase Φ_{rs} (panel a) and SH intensity $I_s^{2\omega}$ (panel b). Solid curves are fits to the data within the model of CP line shapes. Dotted lines are fits with excitonic line shapes for all the resonances.

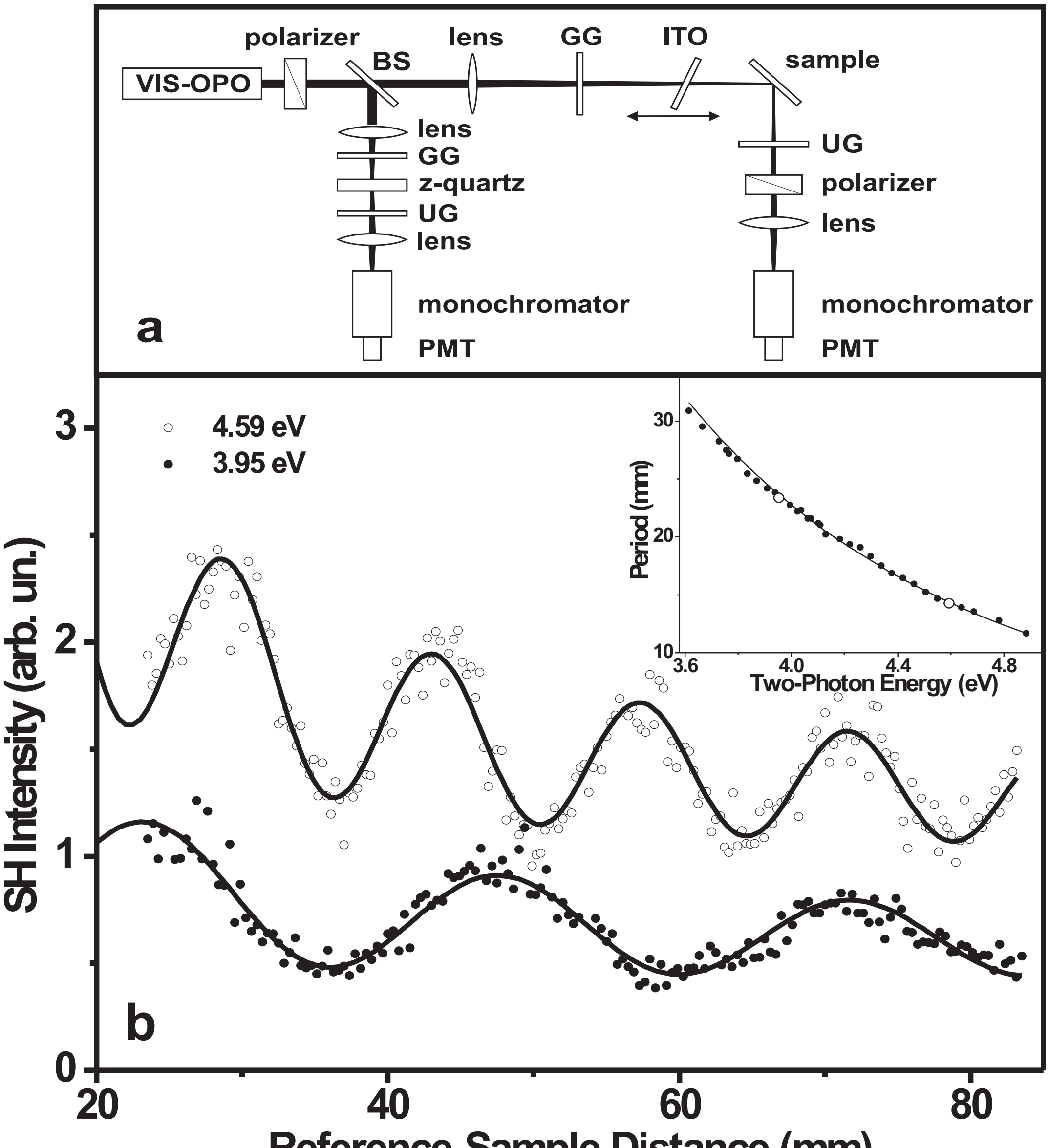

polarizer
BS
lens
GG
ITO
sample
VIS-OPO
lens
GG
z-quartz
UG
lens
monochromator
PMT
UG
polarizer
lens
monochromator
PMT
a
4.59 eV
3.95 eV
SH Intensity (arb. un.)
Period (mm)
Two-Photon Energy (eV)
b
Reference-Sample Distance (mm)

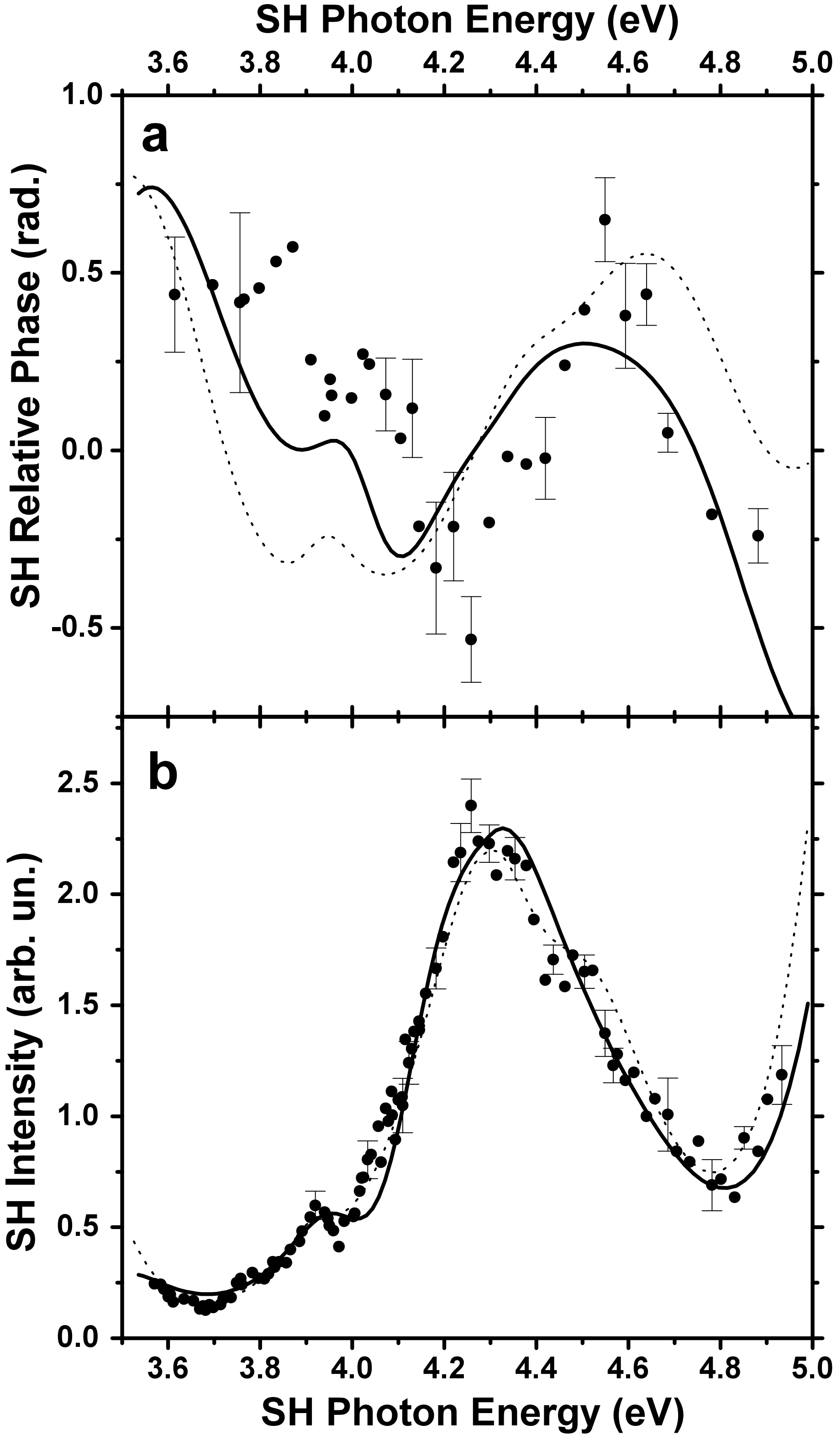

SH Photon Energy (eV)
3.6
3.8
4.0
4.2
4.4
4.6
4.8
5.0
1.0
0.5
0.0
-0.5
a
SH Relative Phase (rad.)
b
2.5
2.0
1.5
1.0
0.5
0.0
SH Intensity (arb. un.)
SH Photon Energy (eV)